Biosensors and Bioelectronics 126 (2019) 240–248

Contents lists available at ScienceDirect

Biosensors and Bioelectronics

journal homepage: www.elsevier.com/locate/bios

Multichannel digital heteronuclear magnetic resonance biosensor

Stephan Huber[a,b,1], Changwook Min[a,c,1], Christoph Staat[b], Juhyun Oh[a], Cesar M. Castro[a], Axel Haase[b], Ralph Weissleder[a,d], Bernhard Gleich[b], Hakho Lee[a,e,*]

[a] Center for Systems Biology, Massachusetts General Hospital, Harvard Medical School, Boston, MA 02114, USA
[b] Munich School of BioEngineering (MSB), Technical University Munich, 85748 Garching, Germany
[c] Harvard-MIT Health Sciences and Technology, MIT, Cambridge, MA 02139, USA
[d] Department of Systems Biology, Harvard Medical School, Boston, MA 02114, USA
[e] Center for NanoMedicine, Institute for Basic Science (IBS), Seoul 03722, Republic of Korea

ARTICLE INFO

Keywords:
Magnetic sensor
Biosensor
Nuclear magnetic resonance

ABSTRACT

Low-field, mobile NMR systems are increasingly used across diverse fields, including medical diagnostics, food quality control, and forensics. The throughput and functionality of these systems, however, are limited due to their conventional single-channel detection: one NMR probe exclusively uses an NMR console at any given time. Under this design, multi-channel detection could only be accomplished by either serially accessing individual probes or stacking up multiple copies of NMR electronics; this approach still retains limitations such as long assay times and increased system complexity. Here we present a new scalable architecture, HERMES (hetero-nuclear resonance multichannel electronic system), for versatile, high-throughput NMR analyses. HERMES exploits the concept of software-defined radio by virtualizing NMR electronics in the digital domain. This strategy i) creates multiple NMR consoles without adding extra hardware; ii) acquires signals from multiple NMR channels in parallel; and iii) operates in wide frequency ranges. All of these functions could be realized on-demand in a single compact device. We interfaced HERMES with an array of NMR probes; the combined system simultaneously measured NMR relaxation from multiple samples and resolved spectra of hetero-nuclear spins (^{1}H, ^{19}F, ^{13}C). For potential diagnostic uses, we applied the system to detect dengue fever and molecularly profile cancer cells through multi-channel protein assays. HERMES holds promise as a powerful analytical tool that enables rapid, reconfigurable, and parallel detection.

1. Introduction

Analytical systems that can reliably, sensitively, and rapidly identify a range of chemical compounds and biomarkers would have broad applications in biomedical research and clinical diagnostics (Giljohann and Mirkin, 2009; Gaster et al., 2011; Abbott et al., 2017; Yeh et al., 2017). Nuclear magnetic resonance (NMR) is a powerful analytical technique valued for its non-destructive detection capability (Lacey et al., 1999; Demas et al., 2009). Most biological samples have intrinsically negligible magnetic susceptibility, causing little interference in NMR measurements (Lee et al., 2015). Even optically turbid samples (e.g., blood, tissue) can be probed by NMR with minimal purification (Haun et al., 2011). Magnetic labeling (e.g., using magnetic nanoparticles) further enhances contrast to biological background for greater sensitivity (Shao et al., 2012) and even makes it possible to measure nanometer-scale distances (Choi et al., 2017). Compared to surface-based magnetic sensors (e.g., giant magnetoresistance or Hall elements) (Issadore et al., 2012; Lee et al., 2017; Ravi et al., 2018) which directly detect individual magnetic objects, NMR-based assays are generally faster for its volumetric sensing nature and can be adopted to characterize chemical structures.

A variety of miniaturized systems have expanded the practical uses of NMR biosensing (Wensink et al., 2005; Lee et al., 2008; Gruschke et al., 2012; Stang et al., 2012; Ha et al., 2014; Peng et al., 2014; Zalesskiy et al., 2014). In addition to improving portability for point-of-care applications, miniaturizing detection systems enhances mass detection sensitivity (Lee et al., 2008), reduces required sample amounts (Olson et al., 1995), and increases signal-to-noise ratio by producing stronger radio-frequency (RF) fields per unit sample volume (Webb, 1997). Indeed, miniaturized NMR systems have been used for single cell profiling, bacterial detection, and highly sensitive protein assays (Haun et al., 2011; Ling et al., 2011; Chung et al., 2013; Peng et al., 2014;

* Correspondence to: Center for Systems Biology, Massachusetts General Hospital, 185 Cambridge St, CPZN 5206, Boston, MA 02114, USA.
E-mail address: hlee@mgh.harvard.edu (H. Lee).
[1] These authors contributed equally.

https://doi.org/10.1016/j.bios.2018.10.052
Received 7 September 2018; Received in revised form 20 October 2018; Accepted 23 October 2018
Available online 27 October 2018
0956-5663/

Jeong et al., 2017). A major drawback of these small systems, however, is their limited throughput and functionality due to a single-channel (SC) detection scheme (i.e., one NMR console per probe). Even with a multi-probe design, most systems essentially execute the SC detection, completing one measurement before proceeding to the next (Wiggins et al., 2009; Gruschke et al., 2012; Kupče, 2013; Ha et al., 2014). Besides its lengthy assay time, the SC detection could experience artifacts arising from different sample dwelling times in NMR probes (e.g., cell settling, analytes interactions with the container). Daisy-chaining multiple transceivers, one for each probe, could be a potential solution for multi-channel (MC) detection; unfortunately, this scheme has limited scalability due to increased system size and complexity (Ogawa et al., 2013).

We herein report the development of a scalable multi-channel microNMR, named HERMES (hetero-nuclear resonance multichannel electronic system). HERMES comprises a programmable NMR transceiver interfaced with an array of NMR probes. We designed various software-defined NMR modules (e.g., T_1 or T_2 relaxometry, NMR spectroscopy) and programmed the transceiver to instantiate these modules and execute them in a time-interleaved manner. This scheme allowed a single transceiver to i) perform versatile NMR detection on-demand and ii) perform simultaneous MC measurements. We also devised an active decoupling network for improved electrical isolation and fast switching among NMR probes. As a proof of concept, we applied HERMES to parallel NMR relaxometry of multiple samples and heteronuclear NMR spectroscopy (1H, 19F, 13C); the HERMES results showed an excellent match with those from separate SC measurements. We further extended HERMES for biomedical applications, performing cancer cell profiling and infection (dengue fever) diagnosis based on multi-marker signatures.

2. Methods

2.1. System setup

We used two permanent magnets, a 0.5 T magnet (PM1055-050N; Metrolab, Switzerland) for NMR relaxometry and a 1 T magnet (M2; Aspect Imaging, Israel) for spectroscopy. The digital processing unit (DPU) was implemented on a ML605 board (Xilinx, USA), which communicated with a computer through a direct Ethernet connection. For signal digitization, we used a FMC150 (Abaco, USA) card. The ADC sampling rate was 245.76 Msps with 14-bit resolution. The DAC sampling rate was 491.52 Msps with 16-bit resolution. The custom-built analog transceiver delivered 21.5 dBm (0.5 T) and 20.5 dBm (1 T) excitation power. Receiver gains were 77 dB (0.5 T) and 74 dB (1 T).

2.2. NMR coil fabrication

The NMR microcoils were wound around 3D-printed hollow cylinders. Every microcoil had 8 turns of a 0.4 mm diameter enameled copper wire. The coil length was 4 mm, and the coil diameter 2.4 mm. The sample volume per coil was 5 μL. The enclosing body coil was 17 mm in length and 12 mm in diameter with 8 windings of a 0.8 mm enameled copper wire. The 90° microcoil pulse lengths were 6 μs (0.5 T) and 8.5 μs (1 T). All coils were mutually orthogonally aligned. The decoupling coils in the matching network were also wound with a 0.56 mm-diameter enameled copper wire. For the 4-channel probe, the decoupling coils had a diameter of 3.5 mm and 29 turns. For the 6-channel probe, the diameter was 5 mm, with 16 coil turns. The center-to-center distances between two adjacent decoupling coils were 7.5 mm (4-channel probe) and 8 mm (6-channel probe).

2.3. Relaxivity measurements

Copper sulfate ($CuSO_4$) was dissolved with Cu^{2+} concentrations ranging from 0.0626 to 313 mM. For the longitudinal relaxivity detection, we measured signals at 16 inversion time (TI) points. We varied TIs according to Cu^{2+} concentrations. For example, at the highest Cu^{2+} concentration, TI values were from 2 to 30 ms; at the lowest Cu^{2+} concentration, TI values were between 5 and 750 ms. All multi-probe measurements had an additional TI ($> T_1$) to ensure proper inversion recovery of samples. Measured data were fitted to an exponential build-up curve $[a_0 - a_1 \cdot \exp(-TI/a_2)]$ wherein a_i ($i = 0, 1, 2$) are fitting parameters. For the transversal relaxivity measurement, we used the 3 ms echo time (TE). Each NMR probe was on for 300 μs to receive excitation pulse, and the corresponding echo signal was sampled for 100 μs. We measured up to 1600 echo signals for each sample. Data were fitted to an exponential decay curve $[a_0 \cdot \exp(-TE_n/a_1)]$ with two fitting parameters (a_0, a_1), where TE_n is the n-th echo time. To determine the relaxivities out of the recorded relaxation rates a robust least square fit with bisquare weights was employed. All experiments were performed at an ambient temperature of 22 °C with 10 repetitions.

2.4. Heteronuclear resonance spectroscopy

The ^1H Larmor frequency from the H_2O channel was used as a frequency reference. We used the multiplication factors (Harris et al., 2002) 0.94094011 for ^{19}F and 0.25145 for ^{13}C. To improve the B_0 homogeneity, the shim unit of the 1 T magnet was turned on. Samples for the 1H probes were water (H_2O), N,N-Dimethylformamide (C_3H_7NO), glycerol ($C_3H_8O_3$), and 1-propanol (C_3H_8O). For the ^{19}F probes, we used 2,2,2-trifluoroethanol ($C_2H_3F_3O$) and perfluoro-1,8-dichlorooctane ($C_8Cl_2F_{16}$). For the ^{13}C experiment, we used an enriched urea (8 M) dissolved in D_2O/H_2O.

2.5. Preparation of carboxylated polystyrene beads

3 mg of polystyrene beads with carboxyl groups (3 μm, Polysciences) were suspended in 100 μL of 0.1 M MES (2-(N-morpholino) ethanesulfonic acid) buffer (28390, Thermofisher). The beads were mixed with 2 mg of EDC (22980, Thermofisher) and Sulfo-NHS (24520, Thermofisher) in 0.1 M MES buffer (50 μL) and incubated (20 min, 20 °C). After incubation, the NHS-EDC coupled beads were triple washed with PBS using 0.45 μm centrifugal filter (3000 rpm, 1 min) and resuspended in 100 μL PBS. 100 μg of affinity ligands against target proteins were added and mixed thoroughly, and then the whole mixture was incubated (12 h, 4 °C) with slow tilt rotation. The conjugated beads were washed four times with PBS containing 0.05% tween (PBST) and resuspended in 200 μL of 1% BSA PBS solution (PBS +).

2.6. Magnetic assay for protein detection

50 μL of target protein was mixed with 2 μL of ligand-coupled polystyrene beads (see Supplementary Methods) and 48 μL of PBS solution containing 1% BSA and 0.05% tween (PBST +), and the mixture was incubated for 30 min at room temperature, washed with PBST three times using 0.45 μm centrifugal filter for 1 min at 3000 rpm (UFC30HV00, EMD Millipore), and resuspended in PBST. The target-captured beads were then mixed with 10 μL of biotinylated antibodies of interest (10 μg/mL) and incubated for 30 min at room temperature. After incubation, the antibody-bound beads were washed and re-suspended in PBST (100 μL). The washed beads were mixed with 2 μL of streptavidin modified magnetic nanoparticles (1.0 mg [Fe]/mL, 30 nm, SHS-30-01, OceanNanoTech) and incubated for 20 min at room temperature. The MNP-coated beads were washed with PBST and reconstituted in PBS (10 μL).

2.7. Cancer cell labeling

An ovarian cancer cell line (OvCAR3) was maintained in RPMI 1640 medium with 10% fetal bovine serum (Atlas Biologicals, S12450),

supplemented with L-glutamine 1× (Corning Mediatech, 25-005-CI). Cells were cultured in a standard humidified incubator (37 °C, 5% CO_2). Next, cells were detached from the culture dish by trypsin with 0.05% EDTA (Corning Mediatech, 25-052-CI) before labeling with MNPs. Cancer cells were first washed with PBS and then fixed with a 3:1 PBS and paraformaldehyde mixture for 20 min at room temperature. The fixed cells were washed and blocked with a blocking buffer (1% BSA with PBS) for 30 min at room temperature. The washed cells were incubated with antibody-biotin conjugates (5 μg/mL, 1% BSA with PBS) for 30 min and washed via centrifugation (350 ×*g*, 5 min). Finally, cells were mixed and incubated with magnetic nanoparticles (1.0 mg[Fe]/mL, 30 nm, SHS-30–01, OceanNanoTech) for 30 min at room temperature, then washed 3 times via centrifugation (350 ×*g*, 5 min). All labeling experiments and measurements were performed at least three times.

3. Results and discussion

3.1. System architecture

HERMES employs a time multiplexing technique to realize the multi-channel (MC) NMR (Fig. 1A). The system generates a serialized stream of MC excitation pulses and feeds them to an array of NMR probes connected to a channel selector. Through synchronous switching, the selector redistributes these pulses to each probe, constructing an excitation sequence for parallel measurements. After each pulse, the resulting NMR signal is recorded, and all signals are digitally arranged into full NMR responses from the array. This time-sharing concept enables parallel measurements of longitudinal (T_1) and transverse (T_2) relaxation as well as NMR spectroscopy within a single NMR console.

We implemented the MC algorithm using a software-defined radio (SDR) strategy (Fig. 1B). By programming a digital processing unit (DPU), we constructed a stack of virtual NMR modules that are conventionally built with discrete electronic components. Each module has i) signal sources accompanied by a switch for pulse generation and ii) two heterodyne receivers to process NMR signals, one for in-phase and the other for the quadrature phase. The DPU also contains other functional blocks, including multiplexers to control communications with NMR modules, internal data storage, and a microcontroller. We interfaced the DPU with a NMR probe array through a single-channel analog transceiver with a variable gain. The SDR approach has several advantages. First, the system can be easily scaled up without hardware modification. Under this design, a complete NMR system is defined by a virtual NMR module, a shared transceiver, and a NMR probe; a new NMR channel can be added by spawning a virtual module inside the DPU and connecting a probe. Second, the same NMR console can be used to detect heteronuclear signals at different NMR-field strengths simply by changing an operation parameter (i.e., the frequency of the signal generator).

Fig. 1C shows a HERMES prototype. We used a field-programmable-gate-array (FPGA) board as a DPU and custom-designed an analog transceiver. We constructed three sets of NMR probes: a 2-channel array for ^{13}C NMR, a 4-channel array for ^{1}H NMR with a portable magnet (0.5 T), and a 6-channel array for NMR spectroscopy (^{1}H, ^{19}F) with a large magnet (1.0 T).

3.2. NMR probe design

A key design factor for MC detection is to minimize crosstalk among probes at the Larmor frequency (f_0). To achieve this goal, we devised an active detuning scheme; at a given time, only one selected NMR probe

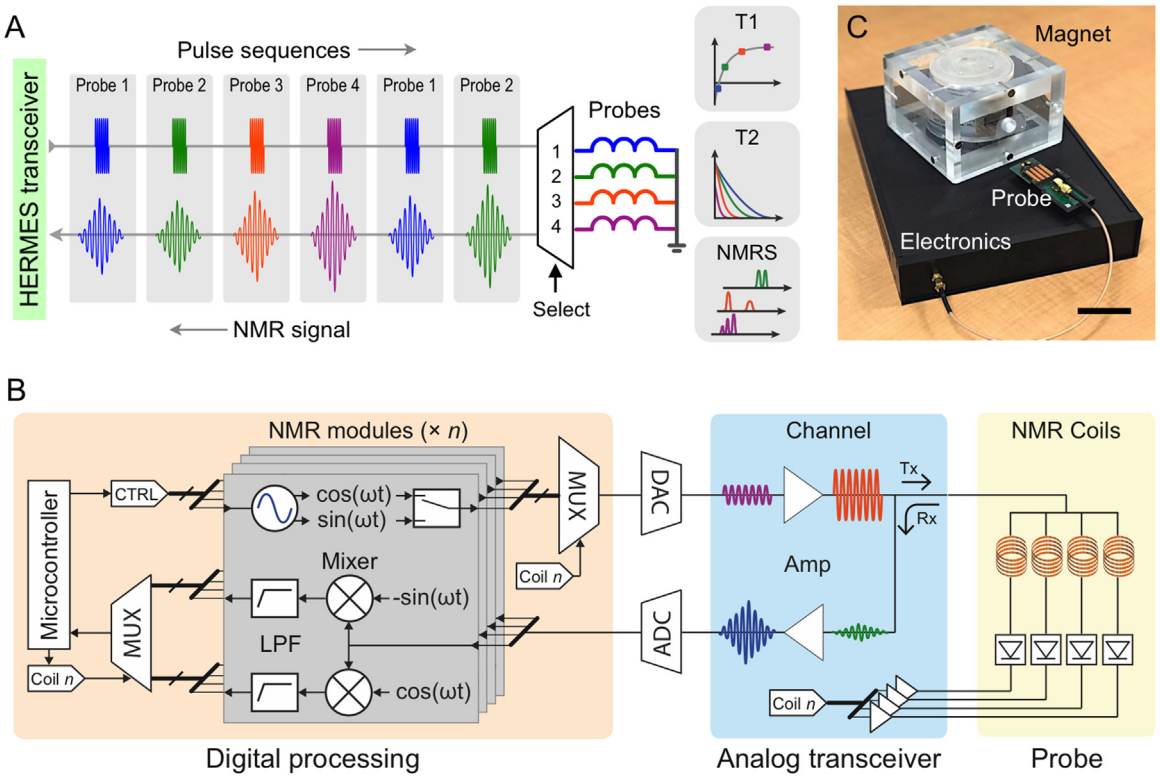

Fig. 1. *Heteronuclear resonance multichannel electronics system (HERMES).* (A) A high-speed transceiver is time-shared with an array of NMR probes. The transceiver modulates parallel excitation pulses into a time-interleaved sequence. The resulting NMR signal stream is digitally demodulated. The scheme enables multimodal, parallel NMR detection. (B) Virtual NMR modules are programmed inside the digital signal processor with each module independently tuned for a different NMR frequency and/or measurement types (e.g., T_1 or T_2 relaxometry, NMR spectroscopy). New NMR modules can be created on demand without hardware modification, providing a cost-effective and scalable approach to multiplexed NMR detection. (C) HERMES prototype. The system consists of a portable magnet, an NMR probe array, and a digital transceiver (black box). Scale bar, 5 cm.

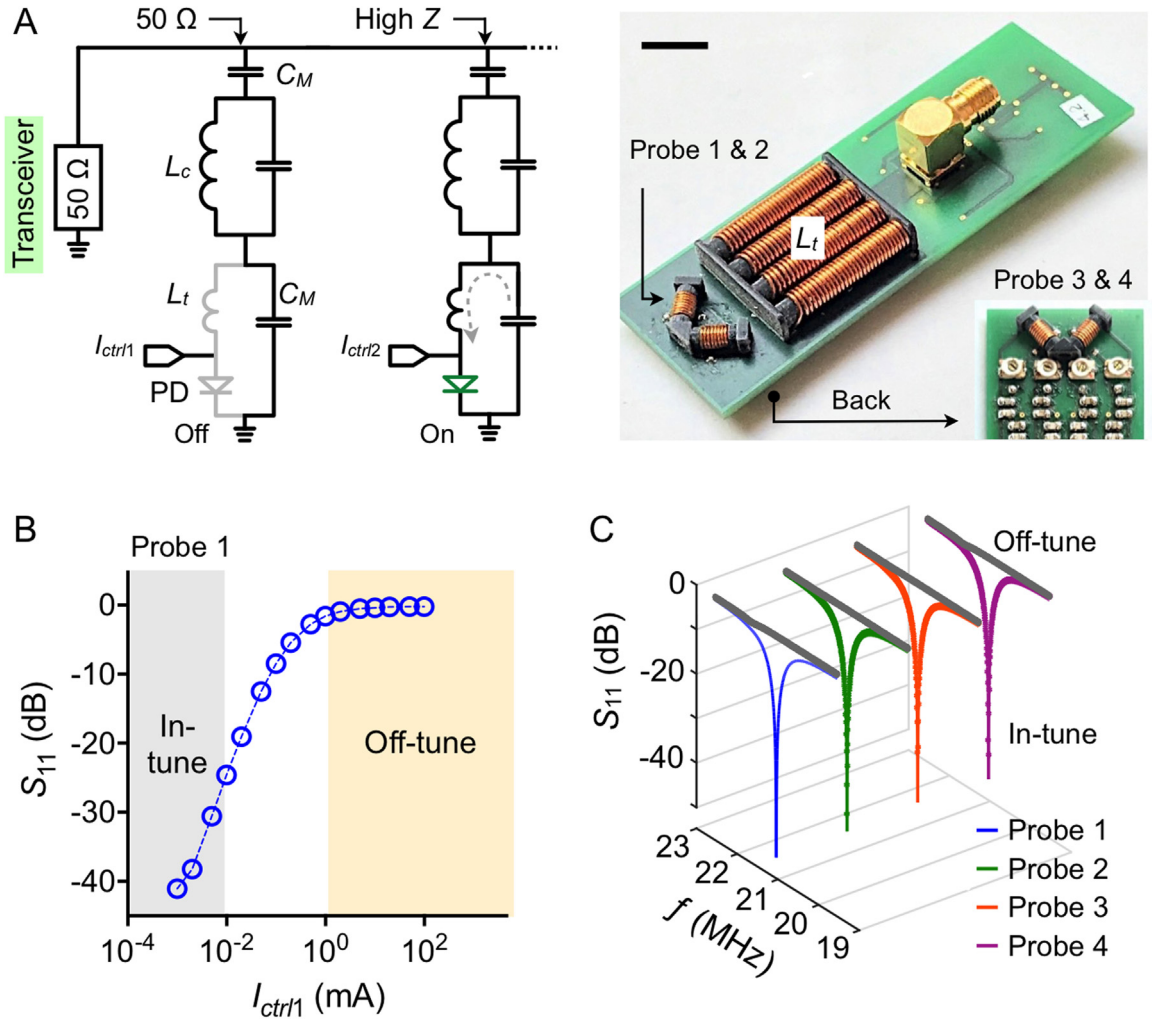

Fig. 2. *NMR-probe selection network.* (A) An active detuning network. (Left) Each NMR coil (L_c) is connected to transceiver ports through matching capacitors C_M. The ground-side capacitor has an additional inductor (L_t) and a PIN diode (PD) in parallel. When the diode is "off", the probe is 50 Ω-matched. With the diode "on", L_t and C_M form a resonant tank with high impedance, which effectively decouples the probe from the transceiver. (Right) A photo of 4-channel NMR probes with the active detuning circuits. The sample volume of each probe was 5 μL. Scale bar, 1 cm. (B) The scattering parameter (S_{11}) of an NMR probe in (A) was measured while sweeping the bias current to a PIN diode. With the diode in the off state, the NMR probe was impedance-matched (50 Ω), showing low reflection (S_{11} = −47 dB). Turning the diode on significantly increased the reflection (S_{11} = −0.24 dB). (C) Scattering parameters of the 4-probe array were measured, with a single probe selected at a given time. Only a selected probe showed low S_{11} (colored profiles), and the rest of the unselected probes had high reflection (gray profiles).

was impedance-matched (50 Ω) to the analog transceiver, while the rest of probes were assumed to have high impedance ($|Z|$ = 3.4 kΩ). We constructed an NMR probe, based on a differential matching network, consisting of an NMR coil and three capacitors (Fig. 2A). To enable active detuning, we added an inductor (L_t) and a PIN diode in parallel with a grounding capacitor (C_M) (Mispelter et al., 2006). When the PIN diode is negatively biased, it has high resistance ("off" state); the NMR coil thereby bypasses L_t and connects to the ground through C_M, forming a complete 50-Ω network (i.e., impedance matched at f_0). Conversely, with the diode on, L_t and C_M form a "tank" circuit that has high impedance at the resonant frequency $f = (4\pi^2 \cdot L_t \cdot C_M)^{-1/2}$. Choosing $L_t = (2\pi f_0)^{-2} \cdot C_M^{-1}$ (i.e., $f = f_0$) places the probe in a high-impedance state.

We first validated this scheme using a single NMR probe designed for f_0 = 21.04 MHz. We measured the scattering (S) parameters while sweeping the bias current (I_{ctrl}) to a PIN diode (Fig. 2B). At I_{ctrl} = 100 mA, the probe reflected most of the radio frequency (RF) input (S_{11} = −0.24 dB), effectively disconnected from the transceiver. When the diode was off (I_{ctrl} = 0 mA), the probe had very low reflection (S_{11} = −47 dB), indicating 50-Ω matching to the RF source. We next expanded the method to NMR probe arrays. We programmed HERMES to impedance-match one probe and detune the rest. Fig. 2C shows the S_{11} characteristics of a 4-probe array. Each NMR probe, when selected for impedance match, showed a resonance profile similar to the single probe. Concurrently, all detuned probes maintained high impedance; the isolation between two adjacent probes was > 50 dB. The delays in switching between probes were much shorter (< 5 μs; Fig. S1) than the typical time scale for NMR measurements. Combined with high isolation among probes, these properties enabled virtual parallel detection: probes could be rapidly polled one at a time for NMR excitation and signal reception.

3.3. Multiplexed measurements of longitudinal relaxation

We first configured HERMES for multiplexed T_1 relaxation measurements. We programmed the system to operate in a time-interleaved inversion recovery (TIIR) mode (Fig. 3A): each probe received a pair of 180° (π) inversion and 90° (π/2) reading pulses that were separated by a defined time delay (i.e., inversion time; *TI*); the application of pulse pairs was interleaved to shorten the measurement time. These steps were then repeated after the sample recovery time (T_R) to capture the full T_1 relaxation of samples.

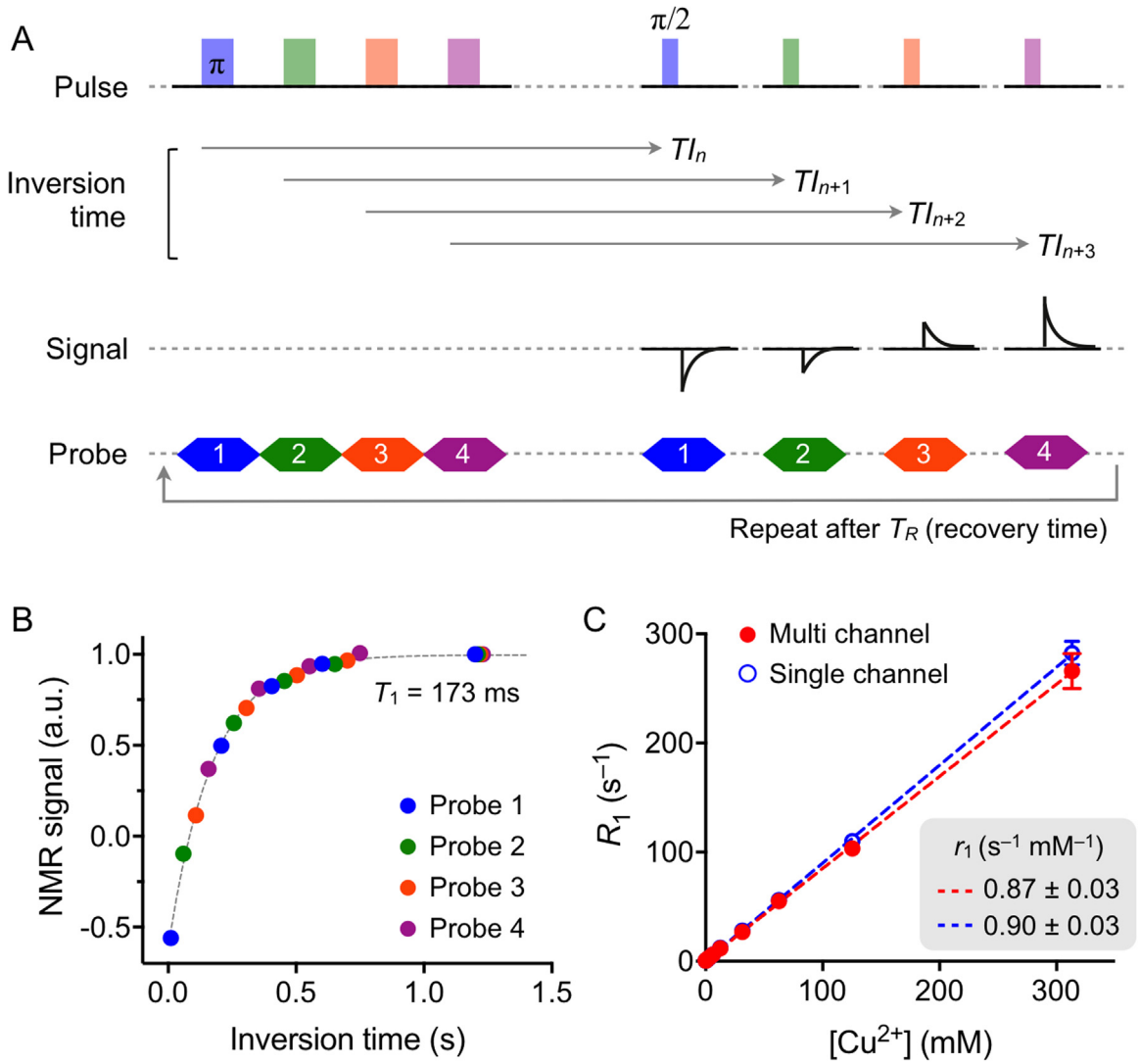

Fig. 3. *Parallel inversion recovery (IR) measurements.* (A) To speed up T_1 measurements, we designed a pulse sequence for time-interleaved inversion recovery (TIIR). A series of inversion (180°; π) pulses was applied to an NMR probe array, 1 pulse per probe. After programmed delays (TI_n, inversion times), NMR signals were read out by applying 90° (π/2) pulses. These sequences were then repeated after the sample recovery time (T_R). (B) Multichannel T_1 measurement of a Cu^{2+} solution. Sample aliquots were loaded to a 4-channel NMR probe. The TIIR measurement acquired multiple data points (color coded) at different inversion times to make the full T_1 relaxation curve. (C) Solutions with varying Cu^{2+} concentrations were measured by the conventional IR (a single probe) and the TIIR (4 probes) methods. The observed longitudinal relaxivity (r_1) values matched.

To test the parallel T_1 detection, we loaded NMR probes with aliquots from a single Cu^{2+} solution and performed the TIIR measurements. With the 4-channel probe, we could acquire 20 data points at different inversion times (Fig. 3B) by applying five pulse trains. The measured relaxation time (T_1 = 173 ms) matched with the result (T_1 = 170 ms) from a single probe (Fig. S2). The MC-NMR, however, allowed for faster T_1 determination, because i) four data points at different inversion times were concurrently measured, and ii) the number of waiting periods (T_R) between two consecutive IR was reduced (see Fig. S3). We further varied the Cu^{2+} concentration and measured the corresponding relaxation rate (Fig. 3C). The longitudinal relaxivity (r_1) values between the TIIR (multi-channel) and the conventional inversion recovery (single channel) modes were well-matched; the measured values agreed with theoretical prediction (r_1 = 0.89 mM^{-1} s^{-1}; see Supplementary Note).

3.4. Multiplexed measurements of transverse relaxation

We next configured HERMES for multiplexed T_2 relaxation measurements. We designed a pulse sequence for time-interleaved spin-echo (TISE) measurements (Fig. 4A): following the sample excitation with 90° (π/2) pulses, HERMES read our spin echoes effectively in a parallel fashion from all probes. Unlike the TIIR mode, we used two quadrature RF sources (Fig. 1B) to enable CPMG detection, thus compensating for the field inhomogeneity of the NMR magnet. To validate the approach, we loaded the NMR array with samples of varying Cu^{2+} concentrations and applied the TISE pulse sequence. Fig. 4B shows a signal stream from four NMR probes. The full T_2 profiles, concurrently measured with HERMES, are shown in Fig. 4C. By fitting the decay curve of each sample, we obtained the T_2 relaxation time; the measured values matched with those from single-channel NMR of individual samples (Fig. S4). With HERMES in the TISE mode, we could quickly (≈15 s) determine the transverse relaxivity (r_2) of the sample (r_2 = 1.00 ± 0.04 s^{-1} mM^{-1}; Fig. 4D), which agreed with the theoretical value of 0.99 s^{-1} mM^{-1} (Supplementary Note).

3.5. Multichannel hetero-NMR spectroscopy

With its fast digital switching, HERMES could independently operate each NMR probe at different frequencies. We reasoned this

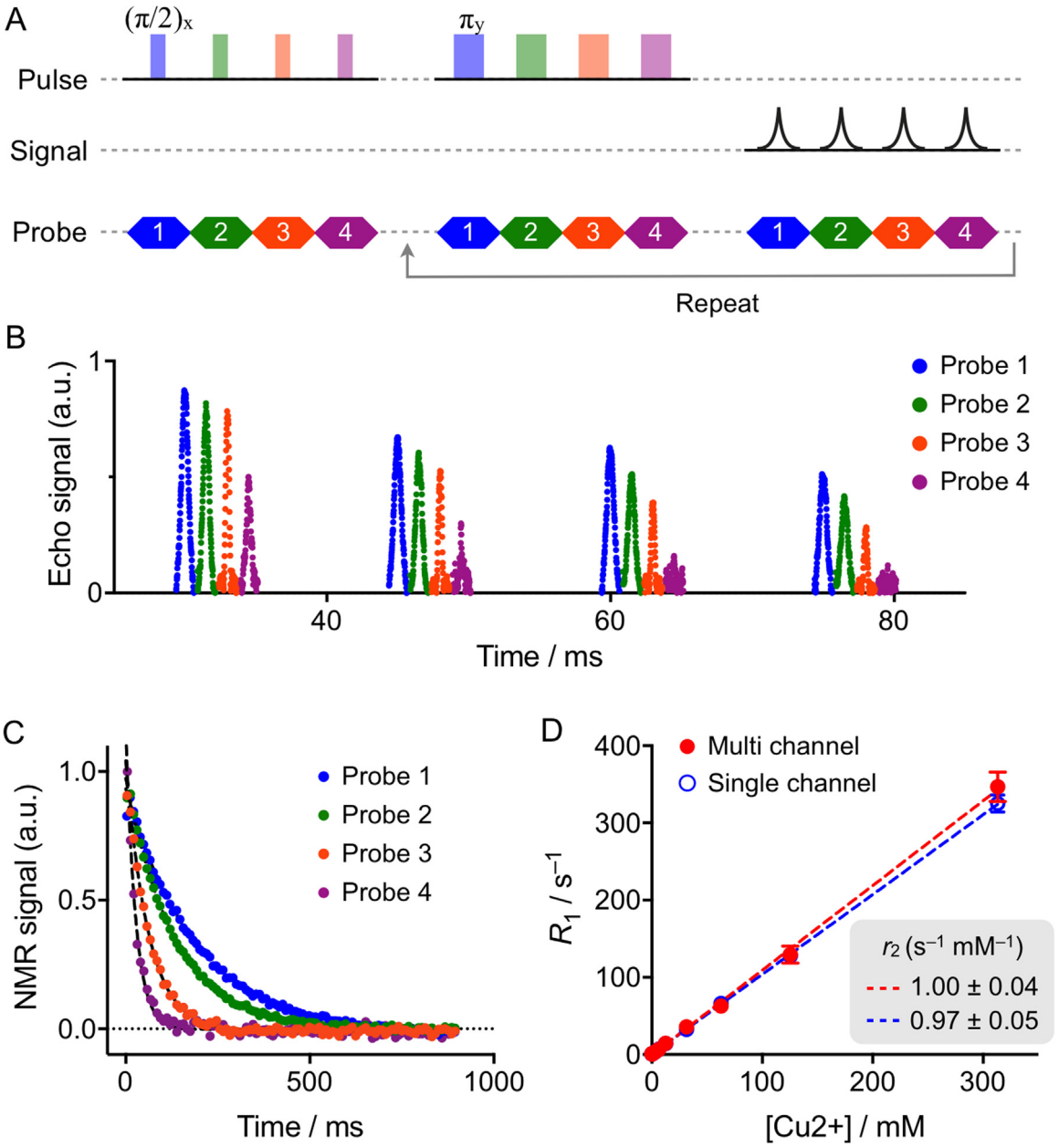

Fig. 4. *Multiplexed T_2 measurements.* (A) A time-interleaved spin-echo (TISE) sequence for parallel T_2 detection. This sequence executed the concurrent CPMG detection among multiple NMR probes. (B) Samples with different Cu^{2+} concentrations were loaded to a 4-channel probe and measured in the TISE mode. A snapshot of the first 4 spin-echo envelopes are shown. (C) HERMES simultaneously reconstructed the full T_2 profile of four samples with different Cu^{2+} concentrations (probe 1, 3.1 mM; probe 2, 6.3 mM; probe 12.5 mM; probe 4, 31.3 mM). (D) The transverse relaxivity (r_2) of Cu^{2+} was measured using the TISE (4 probes) and a single CPMG (1 probe) sequences. Both methods reported statistically identical values ($n = 4$; $P = 0.28$, two-sided t-test).

capacity can be exploited to perform parallel hetero-NMR spectroscopy (h-NMRS) on different chemical species. To prove this concept, we implemented a 6-channel probe (Fig. S5); four coils were tuned for ^{1}H (f_0 = 44.790 MHz) and the rest for ^{19}F (f_0 = 42.135 MHz) at the external magnetic field of B_0 = 1.05 T. One of ^{1}H coils was loaded with H_2O, and its NMR spectrum was used to set the reference for chemical shift. Fig. 5A shows the multi-channel h-NMRS results. Six consecutive FIDs were recorded with every channel in resonance for 125.5 ms (i.e., the total measurement time was 753 ms). We could resolve the chemical shifts of all molecular groups and assign each peak to a specific molecular structure.

We extended this approach to even larger frequency differences, taking advantage of HERMES' wide bandwidth. We prepared a 2-channel probe wherein a ^{1}H body coil enclosed a ^{13}C microcoil (Fig. 5B). Sample (^{13}C enriched urea) was loaded on the microcoil. The body coil measured ^{1}H NMR signal at f_0 = 44.790 MHz, whereas the microcoil detected ^{13}C signal at f_0 = 11.261 MHz. The large difference in NMR frequency (~33 MHz), compared to the resonance width of each coil (< 1 MHz), allowed us to omit the decoupling network. Reliable ^{13}C detection requires multiple averaging due to the low signal level, which makes it critical to compensate for any drifts in the Larmor frequency. We accomplished this by observing the ^{1}H channel for the field locking (Fig. 5C, left) right before ^{13}C measurement. The cycles were then repeated five times to improve the overall SNR in ^{13}C detection (Fig. 5C, right).

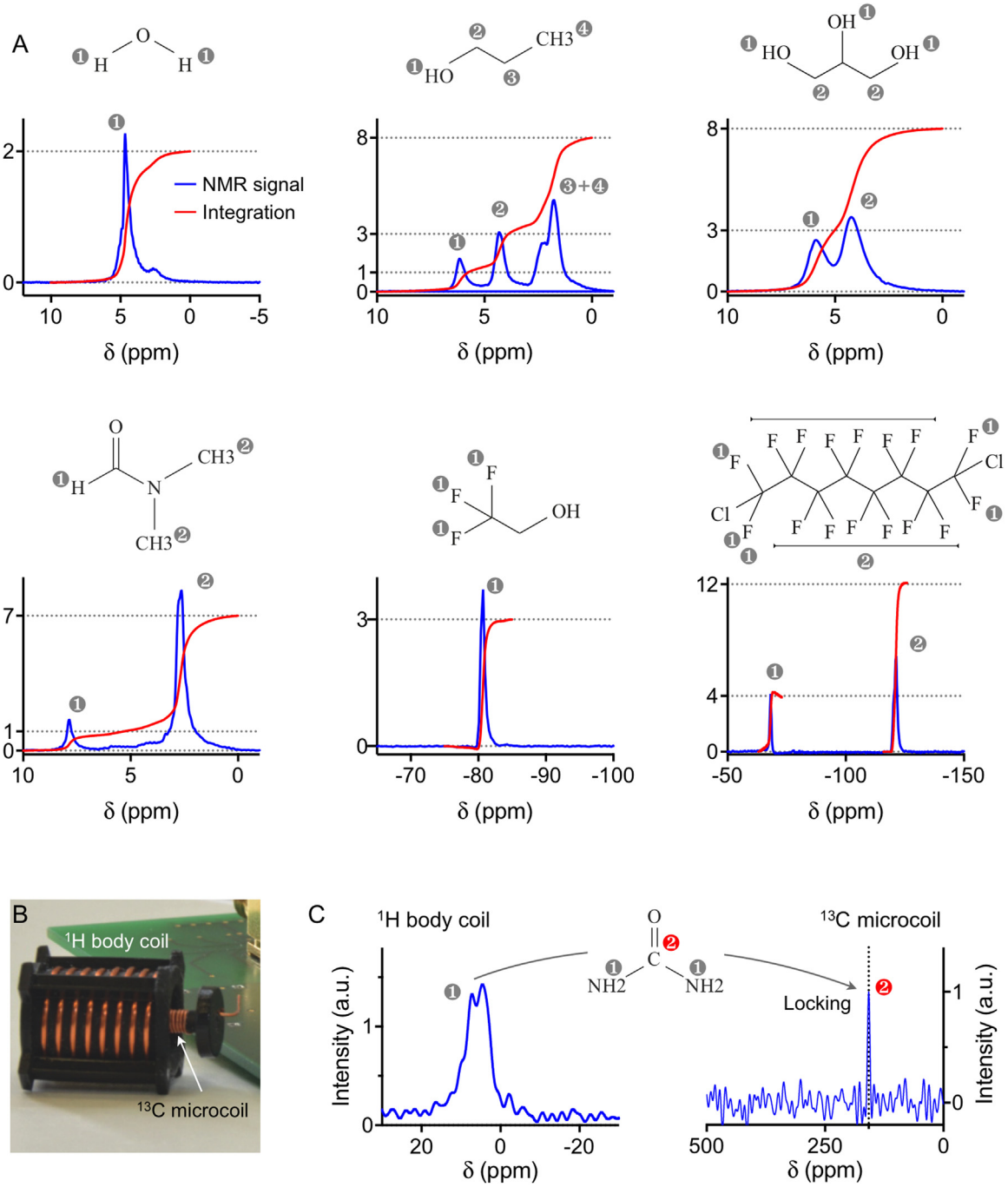

Fig. 5. *Multichannel hetero-NMR spectroscopy (h-NMRS).* (A) HERMES was configured to simultaneously measure the NMRS of different chemical species. A 6-channel NMR probe was designed; 4 channels were tuned for ^{1}H, and the rest for ^{19}F. We tested the following materials: water (H_2O), 1-propanol (top, middle), glycerol (top, right), dimethylformamide (bottom, left), trifluoroethanol (bottom, middle), and perfluorodichlorooctane (bottom, right). Chemical shifts matching with molecular structures were resolved (circled numbers). (B) A 2-channel NMR probe was constructed for field-locked ^{13}C NMRS. The probe had a microcoil (for ^{13}C) enclosed in a body coil (for ^{1}H). (C) NMRS of ^{13}C enriched urea was measured. The body coil measured the ^{1}H spectrum (left); this information was used to compensate for the drift in B_0 (field-locking). The microcoil measured ^{13}C spectra with reference to the locked ^{1}H field (right).

3.6. Biosensing applications

Finally, we applied HERMES to parallel detection of biological targets. We first tuned the system to detect dengue virus (DENV) infection (Bhatt et al., 2013). Accurate DENV diagnosis often requires quantitative, parallel detection of three serological targets (World-Health-Organization, 2009): i) non-structural protein 1 (NS1) DENV antigen, ii) IgM, and iii) IgG antibodies against dengue viral envelope. NS1 protein can serve as a marker for acute dengue infection (< 18 day post onset of symptoms); IgM antibodies appear at the later stage of the infection but persist up to three months; and fold-changes in IgG levels between acute and recovering phases can inform past infection history (primary or secondary).

To detect these soluble markers, we applied the bead-based NMR assay wherein polystyrene microbeads were used as a solid substrate for magnetic labeling. For examples, we captured NS1 protein on polystyrene beads conjugated with antibodies and further labeled NS1 with magnetic nanoparticles (MNPs) conjugated with detection antibodies

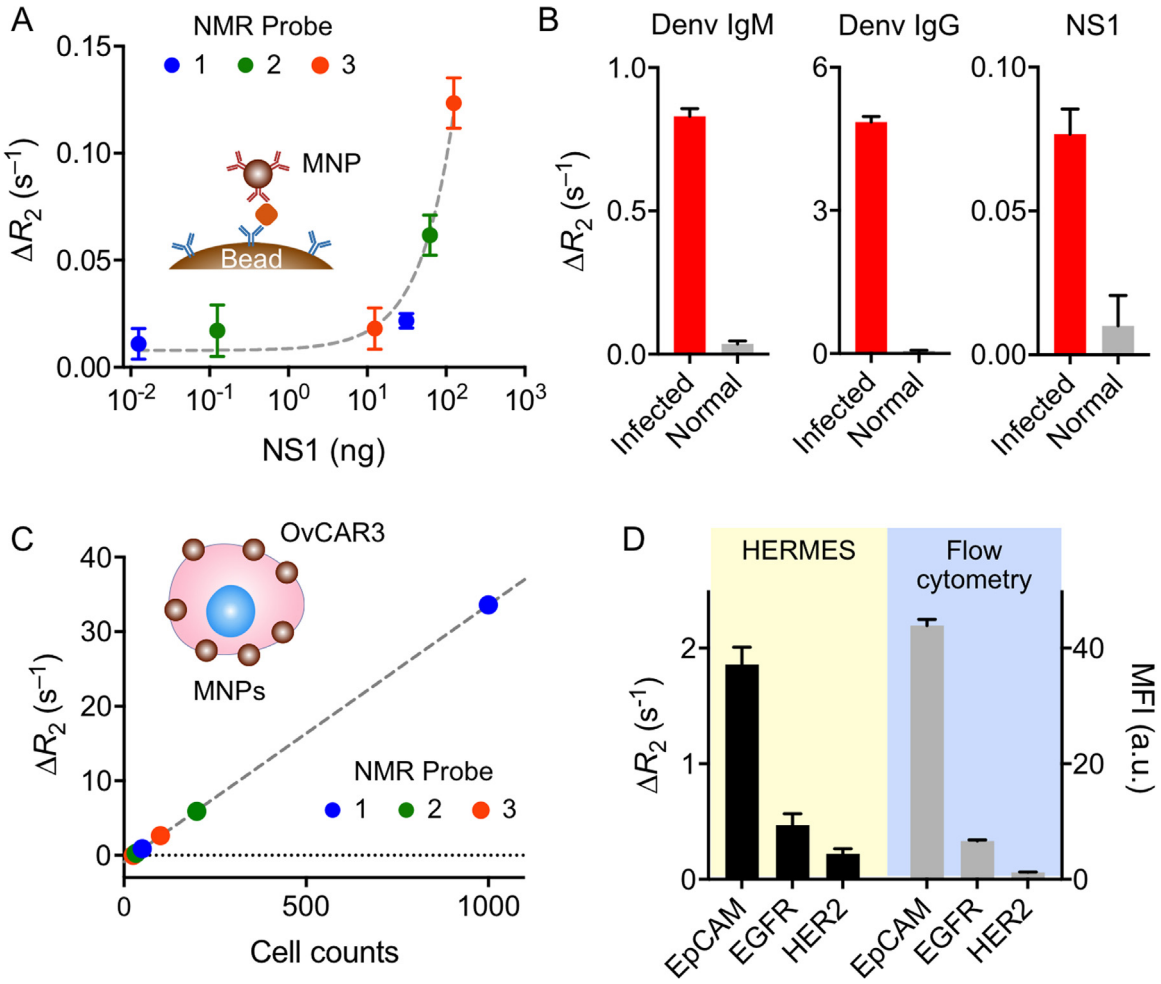

Fig. 6. *Biosensing applications of HERMES.* (A) Titration experiment of dengue virus (DENV) NS1 protein. The target protein was captured on microbeads and labeled with magnetic nanoparticles (MNPs). HERMES measured the transverse relaxation rates ($R_2 = 1/T_2$) of multiple samples simultaneously. The limit of detection (LOD), determined from the 3 × (s.d. of background signal) level, was ~2 pg/μL. Data are displayed as mean ± s.d. from triplicate measurements. The detection limit was ~2 pg/μL. (B) Serum samples mimicking dengue viral infection were aliquoted, and each aliquot was assayed for a target marker (NS1 protein or DENV reactive immunoglobulins). Data are displayed as mean ± s.d. from triplicate measurements. (C) Ovarian cancer cells (OvCAR3) were labeled with EpCAM-specific MNPs; control samples with MNPs conjugated with isotype IgG antibodies. ΔR_2^{EpCAM} ($= R_2^{EpCAM} - R_2^{Control}$) was obtained from multichannel T_2 measurements. The LOD was ~25 cells estimated from the 3 × (s.d. of background signal). Data are displayed as mean ± s.d. from triplicate measurements. The s.d. values are < 0.6 (s^{-1}). (D) Three samples, each containing ~500 cells, were labeled with MNPs specific to EpCAM, EGFR, or HER2; the control (~500 cells) was labeled with isotype IgG-MNPs. The ΔR_2 values were proportional to the marker expression levels. The profiling results accorded well with those by flow cytometry. Data are displayed as mean ± s.d. from triplicate measurements.

(Fig. 6A, inset). Samples were loaded to NMR probes, and parallel T_2 measurements were performed using the TISE mode. We then calculated R_2 changes ($\Delta R_2^{NS1} = 1/T_2^{control} - 1/T_2^{NS1}$). Titration experiments showed that the NMR assay could detect NS1 down to 2 pg/μL (Fig. 6A); this sensitivity was about ten-fold higher than conventional ELISA (Fig. S6). We next performed parallel detection of NS1 and DENV-antibodies (DENV-IgM, DENV-IgG). Mock clinical samples were prepared by spiking all three markers in a human serum sample. Four aliquots (50 μL) of samples were then MNP-labeled for IgM, IgG, NS1, and isotype controls (one marker per aliquot). Parallel HERMES measurements accurately detected these markers (Fig. 6B).

We next performed a cellular assay by labeling cancer cells with molecular-specific MNPs. Cancer cells (OvCAR3, human ovarian carcinoma) were suspended in buffer and serially diluted. Samples were labeled with MNPs by targeting epithelial cell adhesion molecule (EpCAM); cell concentration-matched controls were labeled with MNPs conjugated with IgG antibodies. We then loaded samples, 5 μL each, to the 4-channel NMR probes and measured T_2 values. Fig. 6**C** shows the titration results. The observed R_2 changes ($\Delta R_2^{EpCAM} = 1/T_2^{IgG} - 1/T_2^{EpCAM}$) were linearly proportional to the cell number; the detection limit was ~25 cancer cells. We further profiled cells for multiple biomarkers. Four aliquots were prepared from a single parent sample (cell concentration, 5×10^2 cells/μL). Three aliquots were labeled with MNPs targeting different cancer markers (EpCAM, EGFR, HER2), one marker per aliquot; the fourth was incubated with MNPs conjugated with isotype control antibodies. These samples were assigned to the NMR probe (5 μL per probe) and concurrently assayed. The expression profiles from the parallel NMR agreed with those from flow cytometry (Fig. 6D).

4. Conclusions

Most NMR systems are based on single-channel detection. Applying this design to multichannel detection, either by serially accessing individual probes or stacking up copies of NMR electronics, cannot circumvent limitations of low throughput or increased system complexity. We devised the HERMES strategy as a system-level solution to these issues, expanding NMR's throughput and versatility with minimal cost (see Table S1 for comparison). The key system features are as follows. First, we constructed virtual NMR consoles in the digital domain,

replacing most physical components (e.g., mixers, filters) in the signal path. Modern digital processors can handle data at much higher speed (~1 GHz) than the operation frequency (< 50 MHz) of most portable NMR systems. Such a large bandwidth makes it possible to create multiple virtual NMR consoles and to configure each console to execute different measurement types. Second, we designed an active tuning network to select a specific NMR probe with high isolation. Consisting of all electronic parts (i.e., no mechanical switch), this scalable network is cost-effective and simple, and yet enables fast transition between probes for time-interleaved multiplexing, all digitally controllable.

We implemented a HERMES prototype to prove the concept. We programmed multiple NMR consoles in an FPGA system and interfaced it with an array of NMR probes. By programming pulse sequences, we could perform concurrent T_1 or T_2 measurements on multiple samples. We also detected biological targets (e.g., soluble proteins, cells) labeled with molecular-specific magnetic nanoparticles. Not only did parallel detection reduce assay times, it also improved measurement reliability and integrity; all samples could be consistently handled (e.g., similar dwell times inside sample containers and NMR probes), thus reducing signal artifacts (e.g., T_2 drift caused by cell settling or protein adsorption to sample containers). The hetero-NMR spectroscopy results further exemplified the power of the digital approach. HERMES was readily reconfigured to accommodate system changes, as we could operate each probe at the Larmor frequency specific to a target nuclei. The capacity for parallel spectroscopy provided operational advantages as well. For chemical shift measurements, samples are often mixed with a standard (e.g., tetramethylsilane) to set the frequency reference. In low-field NMR, however, signals from the standard and a sample could be difficult to resolve due to overlapping spectra. Instead, we could use external referencing with HERMES; a standard (e.g., water) was loaded to a probe separate from sample probes, with each probe yielding a clean NMR spectrum from a single compound. Concurrent detection also made it easy to compensate for the errors from temperature drifts and obviated the need for extensive signal processing.

Several technical aspects of this system can be further improved. First, more NMR probes can be added for higher throughput by increasing the homogeneous volume ("sweet spot") of the B_0 field of the permanent magnet. One appealing approach is to adopt the shimmed open magnet, which combines the convenience of the single-sided NMR with high field homogeneity. Second, sample handling could be simplified by incorporating a fluidic structure in the NMR probes. More specifically, embedding microcoils inside fluidic devices could maximize the coil-filing factor and prevent cross-contamination between samples. Third, we could upgrade analog parts (i.e., transceiver, tuning network) to fully exploit the digital counterparts. For example, the current analog transceiver has a bandwidth of ~50 MHz, whereas HERMES already supports $f_0 \sim 125$ MHz ($B_0 \sim 3$ T). By redesigning the transceiver to have a matching bandwidth, HERMES would be compatible with nearly all permanent-magnet NMR systems. The tuning network can also be redesigned to further isolate detuned probes. This will allow us to minimize parasitic signal loss when increasing the number of NMR probes. With such improvements, HERMES could elevate mobile NMR into a powerful analytical tool for high-throughput, versatile analyses of small-volume samples.

Acknowledgements

The authors were supported in part by NIH grants R01-CA229777 (H.L.), U01-CA233360 (H.L.), R01-CA204019 (R.W.), R01-EB010011 (R.W.), R01-EB00462605A1 (R.W.), and P01-CA069246 (R.W.); the Liz Tilberis Award Fund (C.M.C); MGH Scholar Fund (H.L.); Lustgarten Foundation (R.W.); National Research Foundation of Korea (NRF-2017M3A9B4025699, NRF-2017M3A9B4025709; H.L.); the Institute for Basic Science (IBS- R026-D1; H. L.); and the LOTTE Foundation (C.M.). The authors are thankful to C. Hundshammer from the TUM University Hospital rechts der Isar for ^{13}C samples; and K. Joyes for editing the manuscript.

Author contributions

S.H., C.M., A.H., R.W., B.G., and H.L. conceived the research. S.H. and C.M. performed the experiments. S.H. and B.G. developed the device. S.H. and C.S. designed decoupling circuits. J.O. performed flow cytometry. A.H. designed spectroscopy experiments. S.H., C.M., R.W., and H.L. analyzed data. S.H., C.M., J.O., C.M.C., A.H., R.W., B.G., and H.L. wrote the manuscript.

Appendix A. Supplementary material

Supplementary data associated with this article can be found in the online version at doi:10.1016/j.bios.2018.10.052.

References

Abbott, J., Ye, T., Qin, L., Jorgolli, M., Gertner, R.S., Ham, D., Park, H., 2017. Nat. Nanotechnol. 12, 460–466.
Bhatt, S., Gething, P.W., Brady, O.J., Messina, J.P., Farlow, A.W., Moyes, C.L., Drake, J.M., Brownstein, J.S., Hoen, A.G., Sankoh, O., Myers, M.F., George, D.B., Jaenisch, T., Wint, G.R., Simmons, C.P., Scott, T.W., Farrar, J.J., Hay, S.I., 2013. Nature 496, 504–507.
Choi, J.S., Kim, S., Yoo, D., Shin, T.H., Kim, H., Gomes, M.D., Kim, S.H., Pines, A., Cheon, J., 2017. Nat. Mater. 16, 537–542.
Chung, H.J., Castro, C.M., Im, H., Lee, H., Weissleder, R., 2013. Nat. Nanotechnol. 8, 369–375.
Demas, V., Bernhardt, A., Malba, V., Adams, K.L., Evans, L., Harvey, C., Maxwell, R.S., Herberg, J.L., 2009. J. Magn. Reson. 200, 56–63.
G. Webb, A., 1997. Prog. Nucl. Magn. Reson. Spectrosc. 31, 1–42.
Gaster, R.S., Xu, L., Han, S.J., Wilson, R.J., Hall, D.A., Osterfeld, S.J., Yu, H., Wang, S.X., 2011. Nat. Nanotechnol. 6, 314–320.
Giljohann, D.A., Mirkin, C.A., 2009. Nature 462, 461–464.
Gruschke, O.G., Baxan, N., Clad, L., Kratt, K., von Elverfeldt, D., Peter, A., Hennig, J., Badilita, V., Wallrabe, U., Korvink, J.G., 2012. Lab Chip 12, 495–502.
Ha, D., Paulsen, J., Sun, N., Song, Y.Q., Ham, D., 2014. Proc. Natl. Acad. Sci. USA 111, 11955–11960.
Harris, R.K., Becker, E.D., Cabral de Menezes, S.M., Goodfellow, R., Granger, P., 2002. Solid State Nucl. Magn. Reson. 22, 458–483.
Haun, J.B., Castro, C.M., Wang, R., Peterson, V.M., Marinelli, B.S., Lee, H., Weissleder, R., 2011. Sci. Transl. Med. 3 (71ra16).
Issadore, D., Chung, J., Shao, H., Liong, M., Ghazani, A.A., Castro, C.M., Weissleder, R., Lee, H., 2012. Sci. Transl. Med. 4, 141ra92.
Jeong, S., Eskandari, R., Park, S.M., Alvarez, J., Tee, S.S., Weissleder, R., Kharas, M.G., Lee, H., Keshari, K.R., 2017. Sci. Adv. 3, e1700341.
Kupče, E., 2013. Top. Curr. Chem. 335, 71–96.
Lacey, M.E., Subramanian, R., Olson, D.L., Webb, A.G., Sweedler, J.V., 1999. Chem. Rev. 99, 3133–3152.
Lee, H., Shin, T.H., Cheon, J., Weissleder, R., 2015. Chem. Rev. 115, 10690–10724.
Lee, H., Sun, E., Ham, D., Weissleder, R., 2008. Nat. Med. 14, 869–874.
Lee, J.R., Chan, C.T., Ruderman, D., Chuang, H.Y., Gaster, R.S., Atallah, M., Mallick, P., Lowe, S.W., Gambhir, S.S., Wang, S.X., 2017. Nano Lett. 17, 6644–6652.
Ling, Y., Pong, T., Vassiliou, C.C., Huang, P.L., Cima, M.J., 2011. Nat. Biotechnol. 29, 273–277.
Mispelter, J., Lupu, M., Briguet, A., 2006. NMR Probeheads for Biophysical and Biomedical Experiments: Theoretical Principles & Practical Guidelines. Imperial College Press, London.
Ogawa, K., Yokouchi, Y., Haishi, T., Ito, K., 2013. J. Magn. Reson. 234, 147–153.
Olson, D.L., Peck, T.L., Webb, A.G., Magin, R.L., Sweedler, J.V., 1995. Science 270, 1967–1970.
Peng, W.K., Kong, T.F., Ng, C.S., Chen, L., Huang, Y., Bhagat, A.A., Nguyen, N.T., Preiser, P.R., Han, J., 2014. Nat. Med. 20, 1069–1073.
Ravi, N., Rizzi, G., Chang, S.E., Cheung, P., Utz, P.J., Wang, S.X., 2018. Biosens. Bioelectron.
Shao, H., Min, C., Issadore, D., Liong, M., Yoon, T.J., Weissleder, R., Lee, H., 2012. Theranostics 2, 55–65.
Stang, P.P., Conolly, S.M., Santos, J.M., Pauly, J.M., Scott, G.C., 2012. IEEE Trans. Med Imaging 31, 370–379.
Wensink, H., Benito-Lopez, F., Hermes, D.C., Verboom, W., Gardeniers, H.J., Reinhoudt, D.N., van den Berg, A., 2005. Lab Chip 5, 280–284.
Wiggins, G.C., Polimeni, J.R., Potthast, A., Schmitt, M., Alagappan, V., Wald, L.L., 2009. Magn. Reson. Med. 62, 754–762.
World-Health-Organization, 2009. Dengue: Guidelines for Diagnosis, Treatment, Prevention and Control: New Edition. World Health Organization, Geneva.
Yeh, E.C., Fu, C.C., Hu, L., Thakur, R., Feng, J., Lee, L.P., 2017. Sci. Adv. 3, e1501645.
Zalesskiy, S.S., Danieli, E., Blümich, B., Ananikov, V.P., 2014. Chem. Rev. 114, 5641–5694.